ORIGINAL ARTICLE

Influence of Molybdenum Loadings on the Properties of MoO$_3$/Zirconia Catalysts

Femi Francis Oloye[1,2] · Isaac Ayodele Ololade[1]

Abstract

An ideal hydroisomerisation reaction is expected to take place over a bifunctional catalyst, in which a balance between the number of metal sites and acid sites might lead to an optimal performance. In order to assess this relationship and the implications for *n*-heptane hydroisomerisation, various loadings of molybdenum oxide (1–10 wt%) were impregnated on zirconia with a view to producing samples with a range of acid and metal-like properties. The nature and amounts of the acid sites were determined using quantitative FTIR of pyridine adsorption, while the metal-like properties were determined using CO chemisorption. It was observed that zirconia alone contained only Lewis acid sites (1440 cm^{-1}), while addition of MoO$_3$ generated Brønsted acidity (1536 cm^{-1}). The ratio of Brønsted to Lewis acid sites increased with loadings. Similarly, the amounts of CO taken up by the samples increased with MoO$_3$ loadings; hence, the addition of MoO$_3$ resulted in an improved metal like behaviour. The ratio of Brønsted acid to metal-like sites were found to range between 0.009 and 1.180 on going from 1 to 10 wt% MoO$_3$. The materials were used for *n*-heptane hydroconversion. The sample with the highest amount of Brønsted acid site, which also consumed the highest amount of CO showed the highest activity. Hence, it could be concluded that the addition of MoO$_3$ improves the Brønsted acid to metal-like site ratio, which resulted in a pronounced improvement in the activity of the samples.

Keywords Brønsted acid · Metal-like · Hydroconversion · Bifunctional catalyst · Lewis acid

1 Introduction

Solid acid catalysts play a crucial role in the petrochemical industry, where they have largely replaced traditional (liquid) acids, which are active in the liquid phase for hydrocarbon transformations [1]. Common examples of solid acid catalysts of importance in refineries include; zeolites [2], Lewis acid [3], heteropoly acid [2, 4], transition metal carbides [5–9] and zirconia [1, 10–12]. Of recent, there have been renewed interest in the reactivity and chemistry of zirconia based catalyst because of its thermal stability, mechanical properties and its basic, acidic, reducing and oxidizing surfaces [13]. Zirconia is an active catalyst on its own for methanol and hydrocarbon synthesis [2, 14, 15]. However, zirconia performed better when modified with anions such as sulfate, borate, and phosphate and the modified zirconia has been reported to be highly acidic [16–21]. Sulfated zirconia (SZ) had been reported to catalyse isomerisation reactions at low temperature, especially isomerisation of *n*-butane at < 400 K, which requires highly acidic catalysts [17, 19, 20]. Mo has similar effects to sulfate, tungstate and phosphate ions, in modifying the physicochemical properties of unpromoted zirconia [22]. Furthermore, molybdenum or molybdenum oxide over zirconia (MZ) is advantageous compared to SZ, because the catalyst contains no sulfate ions, which can poison the metal sites [2], and can form sulfuric acid at high temperature if there is water in the reaction medium leading to the downstream contamination [23]. However, the acidity-activity relationship has not been well studied for MZ. Furthermore, sulfation alone has been adjudged to

✉ Femi Francis Oloye
pen2crown@gmail.com; femi.oloye@aaua.edu.ng

1 Department of Chemical Sciences, Adekunle Ajasin University, Akungba, Nigeria

2 Surface Chemistry and Catalysis Group, Materials and Chemical Engineering, School of Engineering, University of Aberdeen, Aberdeen AB24 3UE, UK

have little effect on performance [12]. Triwahynono et al. [24] conducted research on n-C_5–C_7 alkane hydroisomerisation over MoO_3–ZrO_2 and Pt/MoO_3–ZrO_2 catalysts and concluded that the catalytic activity of Pt/MoO_3–ZrO_2 was inferior to that of MoO_3–ZrO_2. Brown et al. [12] prepared a series of zirconia-supported molybdenum oxide catalysts with different molybdenum loadings to generate superacidity and observed a marked dependence of Mo content on activity. Reddy et al. [23], recommended further studies to determine the exact nature of the acid sites present on molybdenum zirconia and other oxides. Ruslan et al. [25] concluded that introduction of MoO_3 on ZrO_2 partially eliminated the absorbance band at 1605 cm^{-1} ascribed to Lewis acid sites corresponding to the presence of the monoclinic phase of ZrO_2 and developed several Bronsted and Lewis acid sites with different acidic strengths. MoO_3–ZrO_2 possesses a large number of relatively weak Lewis and Bronsted acid sites as well as strong acid sites. The Mo content and molybdenum oxo species are among the major factors that affects the catalytic activity of Mo/ZrO_2 for n-heptane isomerisation [22]. The isomerisation activity depends on the presence of amorphous Mo species on the tetragonal ZrO_2 surface [22]. Despite the number of works on Mo/ZrO_2 there are dearth of information on the relationship of Brønsted acid to metal-like ratio on conversion. Hence this work will cover area such as quantification of acid sites of different loading of Mo on ZrO_2 and correlating the Brønsted acid to metal-like ratio on conversion.

2 Materials and Methods

2.1 Catalyst Preparation

1.84 g of $(NH_4)_6Mo_7O_{24} \cdot 4H_2O$ calculated based on Mo content was weighed and dissolved in type 1 water (ultrapure deionise water) by stirring with a magnetic stirrer before the addition of 9.0 g of zirconia (stabilised with SiO_2) previously calcined at 773 K for 2 h. It was stirred until all the water had been evaporated (or slurry of the material had been formed). The temperature was regulated and was not allowed to exceed 353 K, and then the sample was dried in an oven at temperature of 383 K. The sample was weighed and calcined for 3 h at 823 K in air flow of 50 mL min^{-1}, after which the sample was allowed to cool to room temperature and stored in a pre-cleaned sample bottle under laboratory conditions and labelled as 10 MZ. Other catalytic formulations were prepared using the same approach, but by varying the amounts of Mo and zirconia to the require contents. The catalysts were labelled as

5 MZ for 5 wt% MoO_3/ZrO_2; 2 MZ for 2 wt% MoO_3/ZrO_2 and 1 MZ for 1 wt% MoO_3/ZrO_2.

2.2 Catalyst Characterisation

The Mo loading was determined using an Agilent 4100 microwave plasma-Atomic emission spectrometer (MIP-AES) after acid digestion in a HCl/HNO$_3$ mixture (the Mo loading was 0.98. 2.01, 4.99 and 10.01 for 1 MZ, 2 MZ, 5 MZ and 10 MZ, respectively). Surface area and porosity was determined using a Micromeritics Tristar instrument after sample pre-treatment in a N$_2$ flow at 473 K for 4 h. X-ray diffraction patterns were recorded on PANalytical X'Pert Pro diffractometer, employing Cu Kα monochromatic radiation. Patterns were collected at room temperature with steps of 0.02° in a range of 20°–80°. The phases were identified with the aid of high score software. Raman spectra were recorded using a Renishaw spectrometer equipped with invia Raman microscope RE 02. 514 nm laser was employed as the exciting source and the measuring parameters were set as follow; accumulation 5, exposure time 10 s and laser power between 50%.

Temperature programmed reduction (TPR) was carried out using a TPDRO 1100 (CE Instruments). Sample was exposed to a gaseous atmosphere composed of 5% H$_2$/N$_2$ at 20 mL min^{-1} and heated from 313 to 1273 K at 10 K min^{-1} then holding this temperature for 40 min. The amount of hydrogen consumed was determined relative to a copper oxide standard. The Langmuir constant and CO chemisorption capacity was determined using a Micromeritics ASAP 2020-C instrument following volumetric estimation of CO uptake as a function of pressure. Pyridine adsorption studies were performed in order to quantify the amounts of Brønsted and Lewis acid sites of all the samples and to specify their strengths. To ensure total coverage of all the acid sites, pyridine adsorption was carried out at ca. 294 K, after sample pre-treatments. Following the recording of a spectrum in the presence of pyridine at room temperature, the samples were subsequently evacuated at 323, 373, 423, 523, 623 and 723 K. The densities of Brønsted and Lewis acid sites were estimated from the integrated absorbance at ca. 1536 and 1439 cm^{-1}. The infrared spectra of the sample were collected using a diffuse reflectance infrared spectrometer cell (Drifts, Perkin Elmer, Spectrum 100) with mercury-cadmium-telluride (MCT) detector at a liquid nitrogen temperature (77 K). The spectra were recorded in the region of 4000–400 cm^{-1} and a resolution of 4 cm^{-1} (see Figure A.3). TG-MS was used to probe the decomposition route of the sample and the possible gases evolved during reaction. The heating rate was set at 283 K min^{-1} from 298 to 1273 K in an air stream (100 mL min^{-1}) (see Figure A.4).

2.3 Catalytic Procedure

Conversion of heptane was carried out with a quartz reactor (1.0 cm internal diameter, 29 cm long) at atmospheric pressure in the presence of hydrogen (0.68 mL min^{-1}). In separate experiments, the effect of space velocity (WHSV) was varied between 0.029 and 0.068 h^{-1}. Reaction temperature was also varied independently between 423 and 823 K. The eluent stream was sampled automatically using an electrically activated ten-port multi-loop VICI Valco sampling valve and samples analysed using a Perkin-Elmer 8410 GC fitted with a 5.6 m long 15% squalene on chromosorb WHP column and FID detector. The conversion (X) was calculated as follow:

$$\%X = \frac{X_i - X_f}{X_i} 100$$

where, X_i is the initial amount (μmol) of heptane before reaction, and X_f is the amount of heptane remaining after reaction.

3 Results and Discussion

3.1 Nitrogen Adsorption–Desorption Studies

The N_2 adsorption–desorption isotherms and pore size distribution for $xMoO_3/ZrO_2$, (where x = 1, 2, 5 and 10) are plotted in Figs. 1 and 2, respectively. The isotherms are type IV. The pore size distribution clearly shows that the materials are predominantly mesoporous material with the majority of points falling between 2 and 50 nm, and few points in the range of micropores and macropores. The derived results from N_2 adsorption–desorption studies are given in Table 1. The surface area of zirconium hydroxide is 374 m^2 g^{-1}, which is reduced to 195 m^2 g^{-1} upon calcination to form zirconia. Calcination results in
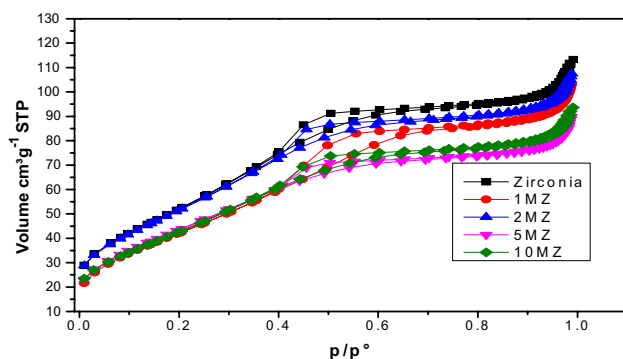

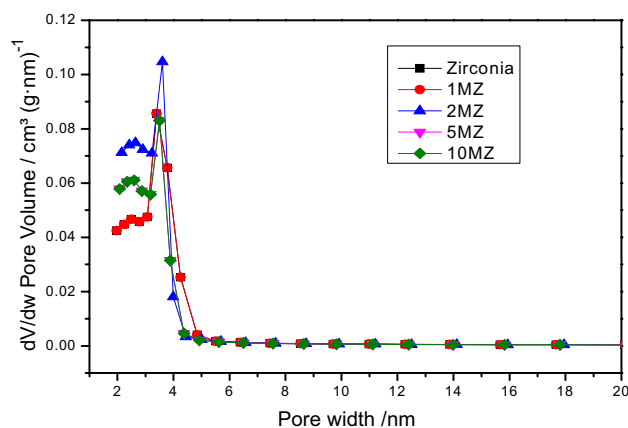**Fig. 1** Nitrogen adsorption–desorption isotherms of zirconia based materials and

Fig. 2 Pore volume distribution of zirconia based materials

a loss of surface area, but addition of MoO_3 increased the surface areas of the materials, and this increased from 127 to 161 m^2 g^{-1} (1–5 MZ), then decreased slightly at higher loadings (10 MZ). The initial increase may be due to the strong interaction between MoO_3 and the support, which inhibits sintering and stabilizes the tetragonal phase of zirconia. Chen et al. [26] also observed increased surface areas with increasing MoO_3 loading up to 20 wt%, and then observed that the surface area decreased at higher loadings. The slight decrease might be due to formation of a crystalline phase of MoO_3 that partially blocks up the pores of the support [22]. High loading of acid enhancer leads to instability of tetragonal zirconia, thus lead to sintering of the materials, which is accompanied by decrease in the surface area [27]. No pronounced difference as the loading of MoO_3 increased was observed in the pore volume and size of the materials. Surface density of MoO_3 on the support is directly proportional to the surface area. The polymolybdate saturation capacity on several metal oxide supports has been reported to be 5 nm^2 approx [28]. Therefore, the maximum loading employed here is below capacity level (Table 1).

Table 1 Physical properties of the ZrO_2 based catalysts

Catalyst	BET (m^2 g^{-1})	Pore volume (cm^3 g^{-1})	Pore size (nm)	ρ_{MoO3}/ (MoO$_3$ atoms nm^2)
Zirconia	195	0.19	3.57	–
1 MZ	127	0.15	3.75	0.32
2 MZ	131	0.16	3.85	0.64
5 MZ	161	0.16	3.92	1.30
10 MZ	158	0.15	3.45	2.65

3.2 XRD

The XRD patterns of xMoO$_3$/ZrO$_2$ are shown in Fig. 3. The diffraction patterns for all samples show features characteristic of the tetragonal phase of ZrO$_2$ with peaks at $2\theta = 30.2°$, 35.1°, 50.1°, 60.28°, and 62.6° [29]. EI-Sharkawy et al. [27] reported that there is critical crystalline size of zirconia below which tetragonal phase is stabilized. Brown et al. [12] and others [22] inferred that the presence of molybdenum in zirconia stabilises its tetragonal phases. No other phases of zirconia were observed in the diffraction pattern, because the calcination temperature and time are the optimum conditions for calcination of zirconia to obtain tetragonal phases [30]. In addition, no phase corresponding to MoO$_3$ or spinel was detected. This may be due to the presence of MoO$_3$ in
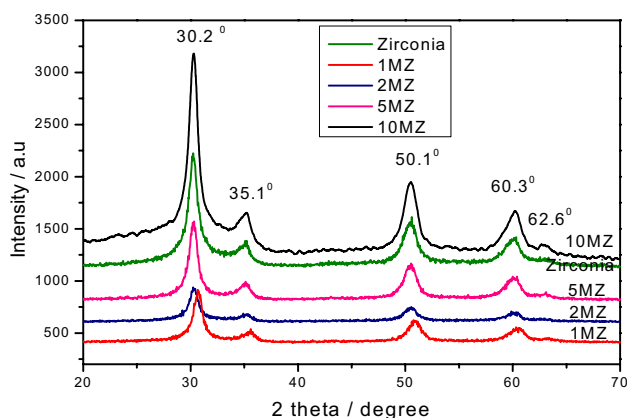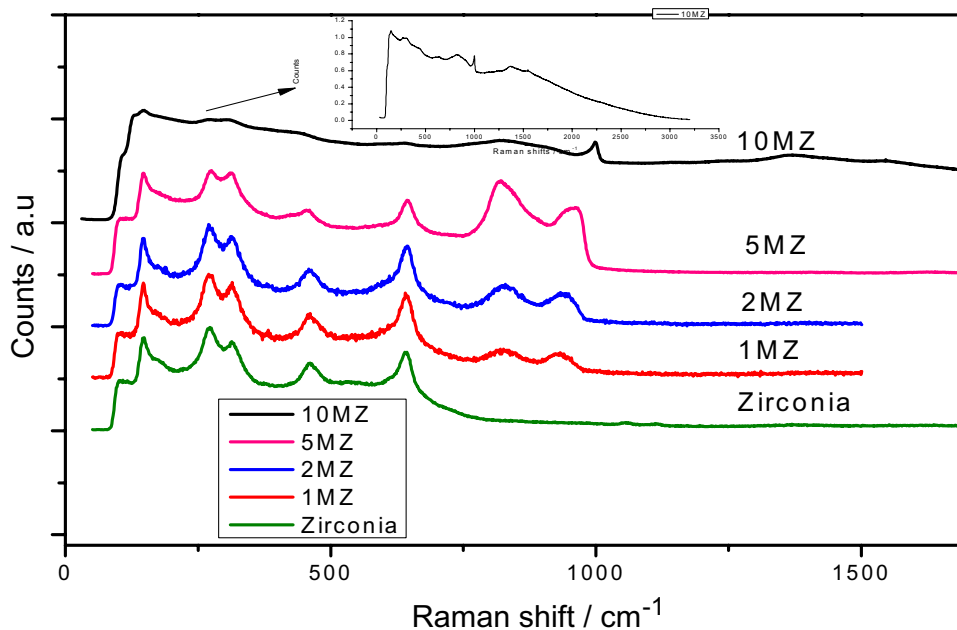
amorphous phase or because MoO$_3$ is present in the range that is too low for detection by XRD [27].

3.3 Raman Spectroscopy

Figure 4 shows Raman spectra of all samples. All the materials exhibited peaks at 100, 147, 274, 313, 416, 646, 830 and 937 cm^{-1}, except for the zirconia, which did not show peaks at ca. 830 and 937 cm^{-1}. Generally, bands at ca. 830 cm^{-1} correspond to Mo–O–Mo vibrations and band at 910-980 cm^{-1} are assigned to Mo=O vibration in two dimensional polymolybdate [12, 31, 32]. The intensity of these two vibrational modes increased with Mo loading. This confirmed that MoO$_3$ species were deposited on the support and that the amount deposited increased with its loadings.

3.4 Pyridine Adsorption Studies

The absorbance band after pyridine adsorption shows both physisorbed and chemical bonded pyridine, which gives an estimation of total acidity. Band intensity on samples treated below 423 K is indicative of total acidity while intensity remaining after evacuation above 423 K is a measure of strong acidity [33, 34]. The term total acidity should not be confused with total acid sites, as the sum of Brønsted and Lewis acid sites are called total acid sites. Typical Brønsted acid sites were observed in the samples, suggesting that pyridine was adsorbed in the form of pyridinium ion at 1635, 1576 and 1536 cm^{-1}, whereas bands suggesting strong Lewis electron pair acceptors sites were observed at 1601 and 1439 cm^{-1} in the samples [35, 36] (Fig. 5). The ratio

Fig. 3 XRD patterns of zirconia based materials

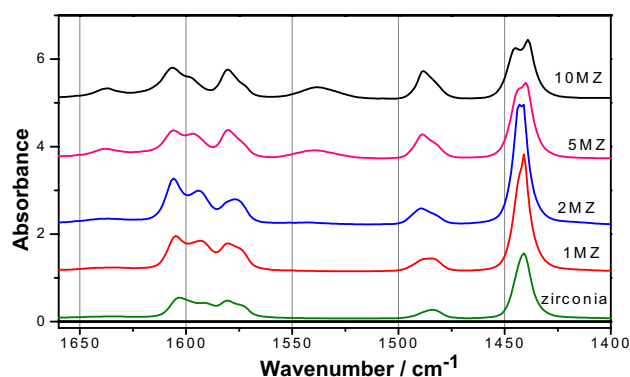**Fig. 4** Example of Raman spectra zirconia based materials

Fig. 5 FTIR pyridine studies on different catalysts

of Lewis to Brønsted acid sites after evacuation at 423 K were 467, 91, 5, and 0.9 for 1 MZ, 2 MZ, 5 MZ and 10 MZ, respectively. Generally, bulk structures of oxides are best described by assuming that they are made up of positive metal ions (cations) and negative O ions (anions). Cations at the surface possess Lewis acidity (i.e. electron acceptors) [37]. The oxygen ions behave as proton acceptors and are thus Brønsted bases. The absorbance at 1488 cm^{-1} contains contributions from pyridine adsorbed at Brønsted and Lewis acid sites. The intensity of the band due to adsorption at Brønsted acid sites at ca. 1536 cm^{-1} increased with MoO$_3$ loading. This intensity was not very substantial for 1 and 2 wt% MoO$_3$, but became very obvious for samples of both 5 and 10 wt% MoO$_3$ (Fig. 5). This observation suggests that MoO$_3$ induces Brønsted acidity on zirconia. The intensities of bands due to both the pyridinium ion and coordinatively bonded pyridine were reduced with subsequent evacuation at increased temperature (Table 2). It is notable that the materials retain adsorbate even after evacuation at 623 K.

The amounts of pyridine retained at Lewis acid site following outgassing below 373 K included contributions from physisorbed pyridine, hence, the significant variation in the quantity of Lewis acid sites for samples 1 and 2 wt% MoO$_3$. The amount of pyridine retained by Lewis acid sites after evacuation at 373 K for 1–5 wt% MoO$_3$ were very similar, but different for that of 10 wt%. In contrary, the number

of Brønsted acid sites increased with loadings. It could be concluded that the strength of Brønsted acid site increased till 523 K, after which the Lewis acid site dominates.

3.5 CO Chemisorption Studies

The CO isotherms on the materials are shown in Fig. 6. All isotherms reach maxima at an equilibrium pressure of ca 200 mmHg. The monolayer volume of CO adsorbed on samples with 1–5 wt% did not show any significant differences, however, the uptake CO on 10 wt% was nearly double that of the others. The large difference between 10 wt% loading and others might be related to the significantly greater amount of molybdenum oxide loaded. The maximum uptakes for all samples and Langmuir constant are given in Table 3. The Langmuir constant increase as a function of the CO uptake. As the Mo loading increase; the extent of interaction between the molybdenum species and the support is reduced. The ratios of Brønsted acid to metal-like sites were 0.009, 0.055, 0.579 and 1.180 for 1, 2 5 and 10 MZ, respectively. Hence, a significant difference would be expected in the catalytic activities of these materials.
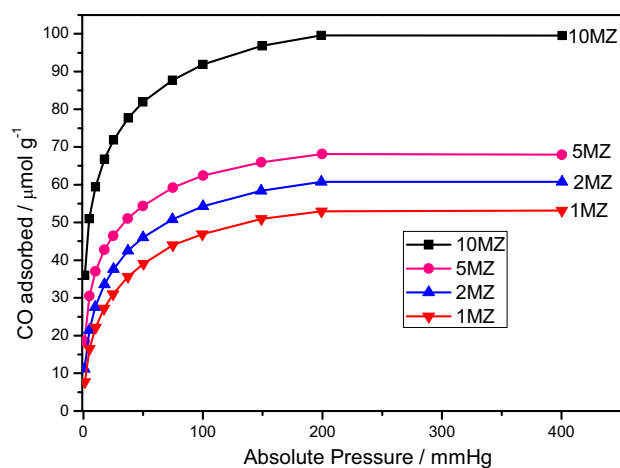

Fig. 6 CO chemisorption on the samples at 308 K after in situ pretreatments

Table 2 Amounts (μmol g^{-1}) of Brønsted acid site (B) and Lewis acid site (L) determined by FTIR of adsorbed pyridine
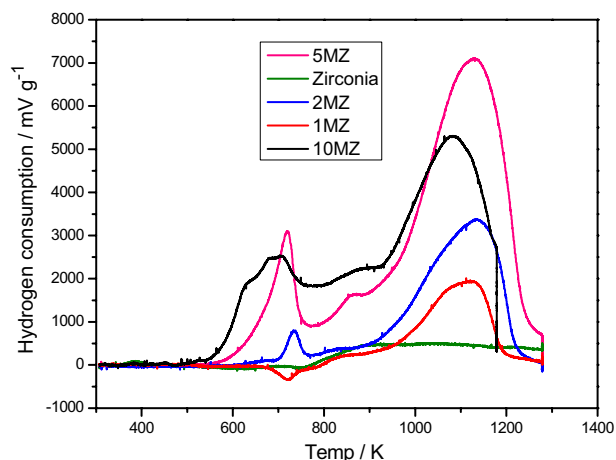
	Adsorption		Desorption									
Temp (K):	293		323		373		423		523		623	
Acid sites	L	B	L	B	L	B	L	B	L	B	L	B
1 MZ	773	0.12	250	1.05	229	0.51	215	0.46	116	0.00	71	0.11
2 MZ	553	4.04	294	3.72	229	3.47	168	1.85	87	0.67	57	0.25
5 MZ	957	26.55	339	36.01	230	40.45	168	31.17	87	3.60	65	0.34
10 MZ	637	133	210	123	131	120	93	99	30	36	22	1.7
5Mo$_2$C/ZrO$_2$	–	–	–	–	160	38	88	48	63	47	38	30

Table 3 Adsorption based properties of the materials

Samples (MZ)	Uptake ($\mu mol\ g^{-1}$)	K $(mmHg)^{-1}$
1	55.50	0.06
2	63.04	0.07
5	69.81	0.10
10	101.69	0.12

Table 4 Extent of MoO_3 reduction on the basis of TPR

Sample (MZ)	H_2 consumed $mmol^{-1}\ g^{-1}$	H_2:MoO_3 ratio
1	0.04	0.18
2	0.49	0.78
5	0.54	0.51
10	1.06	1.12

Fig. 7 TPR profile of all the samples

Fig. 8 Influence Brønsted acid to metal-like ratio on conversion at 723 K and 18 mL min^{-1}

3.6 TPR

The reduction profiles for all samples are shown in Fig. 7. Zirconia did not show any reduction peaks, which mean that this material is difficult to reduce and that any subsequent reduction peaks in other samples, are related to molybdenum species. This observation has been previously reported [31]. However, Eder and Kramer [38] have reported zirconia to reduce from + 4 to + 3 oxidation state in presence of dry H_2. The reduction peaks shifted to lower temperature as the Mo loadings increase (the first peak are 727, 717, 685 for 2 MZ, 5 MZ and 10 MZ, respectively). This is due to the extent of interaction with the support and the ease at which higher loadings are reduced compared to lower loadings. The reduction peak at around 773 K can be assigned to reduction of MoO_3 to Mo_4O_{11} and below 973 K to reduction of Mo_4O_{11} to MoO_2 and above 1073 K to MoO_2 to Mo [39]. The hydrogen consumption increases with loading (Table 4) as expected [10]. Loading below monolayer coverage had been reported to give purely tetrahedral species, which are difficult to reduce due to strong interaction with the support. This explains why the H_2:MoO_3 ratio for Mo loadings below 5 wt% in Table 4 are all less than 1. At moderate loadings, both tetrahedral and octahedral species are present, which are easily reducible [31], while at high loading, octahedral species are dominant. This could possibly explain why some

samples (Table 4) show H_2:MoO_3 ratios are greater than 1. Hence, the higher the MoO_3 loadings, the more reducible it becomes.

3.7 Hydroisomerisation of *n*-Heptane

3.7.1 Effect of Space Velocity and Time on Stream

Figure 8 shows the effect of varying space velocity on the conversion. As expected the conversion decreased with an increase in WHSV (decrease in contact time). Wang et al. [40] concluded that contact time has similar effect as temperature, since an increase in either contact time or temperature will result in an increase in the conversion. Figure 8 also shows the role of molybdenum loadings on the conversion. Higher molybdenum loading delivered increased *n*-heptane conversion. El-Sharkawy et al. [27] attributed an increase in the conversion of cumene dealkylation and ethylene selectivity to increased surface acidity, which was enhanced by increasing loading of MoO_3. Other researchers [31] have reported similar observation. The increase in conversion with MoO_3 loadings might suggest that addition of MoO_3 yields more active sites suggesting dispersion is maintained and has not resulted in the formation of bulk MoO_3 crystallite. The metal crystallite size increase with loading, but

did not result in bulk MoO_3. The surface area and pore size increases in relation to Brønsted acid to metal-like ratio, which increased with conversion, however, the surface area and pore size for 10 MZ were lower compared to others, suggesting that not just one factor influences the conversion, but different catalyst properties. Shimizu et al. [41] observed an increase in *n*-butane isomerisation rates and suggested that this was closely related to the strength of Brønsted acid sites than with the Lewis acid sites. Chica and Corma [15] founds that a linear correlations existed between the number of acid sites and the catalytic activity of the different types of catalytic materials study for *n*-heptane hydroisomerisation. Therefore, the increase in *n*-heptane conversion with loadings might be related to the improvement in Brønsted acid site to metal-like ratio of the materials. No significant difference was observed in the product distributions from using different catalysts for *n*-heptane conversion. This similarity in product distributions might be related to pore volume. Hence, pore volume plays major role in product distributions.

3.7.2 Effect of Temperature

Generally, an increase in temperature will result in an increase in the conversion of *n*-alkanes. This increase in temperature will in most cases at low temperature leads to a concomitant increase in hydroisomerisation products [40, 42, 43]. Hydroisomerisation is expected to follow the conversion up to a maximum, then decrease [40]. Thus, at high temperatures (≥ 723 K), deviations from ideal behaviour will be expected. Figure 9 shows the effect of temperature on the conversion. As anticipated, the *n*-heptane conversion increased with the increase in temperature. However, the activity of 1 and 2 wt% are similar. This may be a consequence of the close similarity in properties of these two samples. The activity of 10 wt% MoO_3 is higher than others, but did not show such significant difference as might have been expected based on the substantial differences in its properties compare to others (Tables 2, 3, Fig. 6).

4 Conclusion

The acidic and metal like properties of MoO_3/ZrO_2 catalysts were tuned by varying different loadings of molybdenum oxide (1–10 wt%) impregnated on zirconia. Calcination of zirconia resulted in a pronounced decrease in surface area, but the loss was compensated by addition of MoO_3. No phases related to molybdenum species could be detected by XRD, suggesting lack of crystallite form of Mo species and/or existence of strong interactions between the supports and molybdenum oxides, leading to highly dispersed phases. The extent of this interaction was found to decrease as the
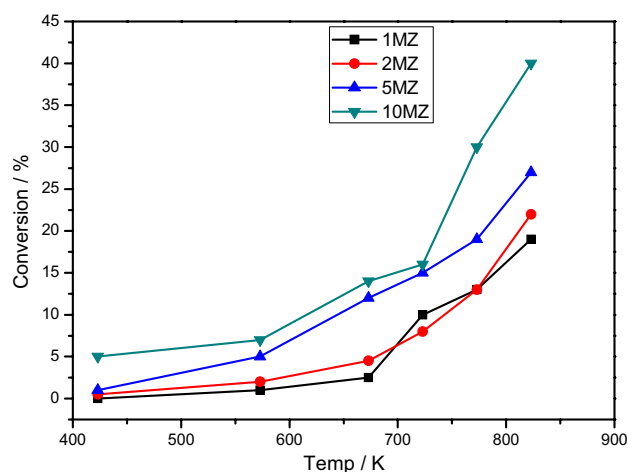

Fig. 9 Influence of varying temperature on conversion of *n*-heptane at 0.06795 h^{-1} and hydrogen flowrate of 18 mL min^{-1}

loadings increased. The presence of molybdenum oxide species in the samples were identified by features due to Mo–O–Mo and Mo=O bonds in Raman spectra. The activity increased as the ratio of Brønsted acid to metal-like sites increased. 10 MZ catalyst with the highest Brønsted acid to metal-like sites ratio gave best hydroconversion of *n*-heptane. This work brings strong supporting evidence that tuning the properties of the catalysts prepared so far could be achieved by simply varying the loading extent of MoO_3 on zirconia.

Compliance with Ethical Standards

Conflict of Interest The author declares that there is no competing interest.

References

1. Oloye FF (2016) Synthesis and characterisation of zirconia supported molybdenum oxide and molybdenum carbide catalysts for hydroconversion of *n*-heptane. PhD thesis, University of Aberdeen
2. Ono Y (2003) A survey of the mechanism in catalytic isomerization of alkanes. Catal Today 81:3–16
3. Galadima A, Anderson JA, Wells RPK (2009) Solid acid catalysts in heterogeneous *n*-alkanes hydroisomerisation for increasing octane number of gasoline. Sci World J 4:1–9
4. Devassy BM, Halligudi SB (2005) Zirconia-supported heteropoly acids: characterization and catalytic behavior in liquid-phase veratrole benzoylation. J Catal 236:313–323
5. Lee JS, Locatelli S, Oyama ST, Boudart M (1990) Molybdenum carbide catalysts 3. Turnover rates for the hydrogenolysis of *n*-butane. J Catal 125:157–170

6. Liu C, Lin M, Fang K, Meng Y, Sun Y (2014) Preparation of nanostructured molybdenum carbides for CO hydrogenation. RSC Adv 4:20948–20954

7. Ham DJ, Lee JS (2009) Transition metal carbides and nitrides as electrode materials for low temperature fuel cells. Energies 2:873–899

8. Lee JS, Oyama ST, Boudart M (1987) Molybdenum carbide catalysts: I. Synthesis of unsupported powders. J Catal 106:125–133

9. Oloye FF, McCue AJ, Anderson JA (2016) Understanding reaction processes for n-heptane over 10Mo₂C/SZ catalyst. Catal Today 277:246–256

10. Galadima A, Wells RPK, Anderson JA (2012) Hydroconversion of n-alkanes over carbided Rh/molybdena zirconia catalysts. Top Catal 55:931–939

11. Arata K, Hino M (1988) Synthesis of solid superacid of tungsten oxide supported on zirconia and its catalytic action for reactions of butane and pentane. J C S Chem Comm 18:1259–1260

12. Brown ASC, Hargreaves JSJ, Taylor SH (1999) A study of "superacidic" MoO₃/ZrO₂ catalysts for methane oxidation. Catal Lett 57:109–113

13. Comelli RA, Vera CR, Parera JM (1995) Influence of ZrO₂ crystalline structure and sulfate ion concentration on the catalytic activity of SO₄²⁻–ZrO₂. J Catal 151:96–101

14. Serra JM, Chica A, Corma A (2003) Development of a low temperature light paraffin isomerization catalysts with improved resistance to water and sulphur by combinatorial methods. Appl Catal A: Gen 239:35–42

15. Chica A, Corma A (1999) Hydroisomerization of pentane, hexane, and heptane for improving the octane number of gasoline. J Catal 187:167–176

16. Arata K, Hino M (1990) Solid catalyst treated with anion: XVIII. Benzoylation of toluene with benzoyl chloride and benzoic anhydride catalysed by solid superacid of sulfate-supported alumina. Appl Catal 59:197–204

17. Hino M, Arata K (1980) Synthesis of solid superacid catalyst with acid strength of Ho ≤ − 16.04. J C S Chem Comm 18:851–852

18. Oloye FF, Alyel R, Anderson JA (2018) Hydroisomerisation of n-heptane over Pt/sulfated zirconia catalyst at atmospheric pressure. Fuel 222(2018):569–573

19. Hino M, Arata K (1995) Synthesis of a highly active superacid of platinum-supported zirconia for reaction of butane. J C S Chem Comm 7:789–790

20. Arata K, Matsuhashi H, Hino M, Nakamura H (2003) Synthesis of solid superacids and their activities for reactions of alkanes. Catal Today 81:17–30

21. Hino M, Kurashige M, Matsuhashi H, Arata K (2006) The surface structure of sulfated zirconia: studies of XPS and thermal analysis. Thermochim Acta 441:35–41

22. Yori JC, Pieck CL, Parera JM (2000) Alkane isomerization on MoO₃/ZrO₂ catalysts. Catal Lett 64:141–146

23. Reddy BM, Sreekanth PM, Reddy VR (2005) Modified zirconia solid acid catalysts for organic synthesis and transformations. J Mol Catal A Chem 225:71–78

24. Triwahyono S, Jalil AA, Ruslan NN, Setiabudi HD, Kamarudin NHN (2013) C5-C7 linear alkane hydroisomerization over MoO₃–ZrO₂ and Pt/MoO₃–ZrO₂ catalysts. J Catal 303:50–59

25. Ruslan NN, Fadzlillah NA, Karim AH, Jalil AA, Triwahyono S (2011) IR study of active sites for n-heptane isomerization over MoO₃-ZrO₂. Appl Catal A Gen 406:102–112

26. Chen K, Xie S, Iglesia E, Bell AT (2000) Structure and properties of zirconia-supported molybdenum oxide catalysts for oxidative dehydrogenation of propane. J Catal 189:421–430

27. El-Sharkawy EA, Khder AS, Ahmed AI (2007) Structural characterization and catalytic activity of molybdenum oxide supported zirconia catalysts. Microporous Mesoporous Mater 102:128–137

28. Xie S, Chen K, Bell AT, Iglesia E (2000) Structural characterization of molybdenum oxide supported on zirconia. J Phys Chem B 104:10059–10068

29. Busto M, Vera C, Grau J (2011) Optimal process conditions for the isomerization–cracking of long-chain n-paraffins to high octane isomerizate gasoline over Pt/SO₄²⁻ZrO₂ catalysts. Fuel Process Technol 92:1675–1684

30. Farcasiu D (1997) Superacidic and bifunctional acid catalysts. ACS Div Petrol Chem 29:745–747 **(preprints)**

31. Chary KVR, Reddy KR, Kishan G, Niemantsverdriet JW, Mestl G (2004) Structure and catalytic properties of molybdenum oxide catalysts supported on zirconia. J Catal 226:283–291

32. Sohn JR, Chun EW, Paet YI (2003) Spectroscopic Studies on ZrO₂ modified with MoO₃ and activity for acid catalysis. Bull Korean Chem Soc 24:1785–1792

33. Khabtou S, Chevreau T, Lavalley JC (1994) Quantitative infrared study of the distinct acidic hydroxyl groups contained in modified Y zeolites. Microporous Mat 3:133–148

34. Bensitel M, Saur O, Lavalley JC, Mabilon G (1987) Acidity of zirconium oxide and sulfated ZrO₂ samples. Mater Chem Phys 17:249–258

35. Devassy BM, Halligudi SB (2006) Effect of calcination on the catalytic activity of zirconia-supported heteropoly acids. J Mol Catal A Chem 253:8–15

36. Corma A (1995) Inorganic solid acids and their use in acid-catalysed hydrocarbon reaction. Chem Rev 95:559–614

37. Chorkendorff I, Niemantsverdriet JW (2007) Concepts of modern catalysis and kinetics, second, revised and enlarged edition. Wiley, Oxford

38. Eder D, Kramer R (2002) The stoichiometry of hydrogen reduced zirconia and its influence on catalytic activity part 1: volumetric and conductivity studies. PCCP 4:795–801

39. de Paiva Jr, José B, Cortez GG, Monteiro WR, Zacharias MA, Rodrigues JA (2007) Characterization and catalytic properties of MoO₃/V₂O₅/Nb₂O₅ in the reaction of decomposition of the isopropanol. In: 2nd Mercosur congress on chemical engineering and 4th mercosur congress on process systems engineering, enpromer

40. Wang Z, Kamo A, Yoneda T, Komatsu T, Yashima T (1997) Isomerization of n-heptane over Pt-loaded zeolite β catalysts. App Catal A: Gen. 159:119–132

41. Shimizu K, Kounami N, Wada H, Shishido T, Hattori H (1998) Isomerization of n-butane by sulfated zirconia: the effect of calcination temperature and characterization of its surface acidity. Catal Lett 54:153–158

42. Galadima A (2012) Development of new and improved catalysts for the isomerization of refinery products. PhD thesis, University of Aberdeen

43. Galadima A, Wells RPK, Anderson JA (2012) n-Alkane hydroconversion over carbided molybdena supported on sulfated zirconia. Appl Petrochem Res 1:35–43